Elastic scattering of ^{25}Al + p to explore the resonance structure in ^{26}Si

H. S. Jung* and C. S. Lee†
Department of Physics, Chung-Ang University, Seoul 156-756, Republic of Korea

Y. K. Kwon, J. Y. Moon, J. H. Lee, C. C. Yun, M. J. Kim, and T. Hashimoto
Institute for Basic Science, Daejeon 305-811, Republic of Korea

H. Yamaguchi and D. Kahl
Center for Nuclear Study (CNS), University of Tokyo, RIKEN campus, 2-1 Hirosawa, Wako, Saitama 351-0198, Japan

S. Kubono, Y. Wakabayashi, and Y. Togano
RIKEN Nishina Center, 2-1 Hirosawa, Wako, Saitama 351-0198, Japan

Seonho Choi and Y. H. Kim
Department of Physics and Astronomy, Seoul National University, Seoul 151-742, Republic of Korea

Y. K. Kim
Department of Nuclear Engineering, Hanyang University, Seoul 133-791, Republic of Korea
and Institute for Basic Science, Daejeon 305-811, Republic of Korea

J. S. Park
Department of Nuclear Engineering, Hanyang University, Seoul 133-791, Republic of Korea

E. J. Kim
Division of Science Education, Chonbuk National University, Jeonju 561-756, Republic of Korea

C.-B. Moon
Faculty of Science, Hoseo University, Asan 336-795, Republic of Korea

T. Teranishi
Department of Physics, Kyushu University, 6-10-1 Hakozaki, Fukuoka 812-8581, Japan

N. Iwasa and T. Yamada
Department of Physics, Tohoku University, Aoba, Sendai, Miyagi 980-8578, Japan

S. Kato
Department of Physics, Yamagata University, 1-4-12 Kojirakawa-machi, Yamagata 990-8560, Japan

S. Cherubini, S. Hayakawa, and G. G. Rapisarda
Laboratori Nazionali del Sud-INFN, Via S. Sofia 62, 95125 Catania, Italy
and Dipartimento di Fisica e Astronomia, Università di Catania, Catania, Italy
(Received 19 May 2014; revised manuscript received 16 July 2014; published 23 September 2014)

Background: The properties of resonances in ^{26}Si are important to better constrain the ^{25}Al$(p,\gamma)^{26}$Si reaction rate relevant to the synthesis of galactic ^{26}Al^{gs} and energy generation in explosive stellar environment at higher temperature.
Purpose: ^{25}Al + p elastic scattering was measured to further constrain and investigate disagreements in resonance parameters for the high-lying excited states of ^{26}Si with high statistics and without background contamination within the target.
Methods: The experiment was performed by bombarding a thick H_2 target with an ^{25}Al radioactive ion beam. The resonances at excitation energies of 6.6–8.3 MeV in the ^{26}Si compound nucleus were studied at the low-energy radioactive-ion beam facility CRIB (Center for Nuclear Study Radioactive Ion Beam separator) at the University of Tokyo.

*Present address: Department of Physics, University of Notre Dame, Notre Dame, IN 46556, USA.
†cslee@cau.ac.kr

Results: Six resonant states were observed and their resonance parameters were extracted by an R-matrix analysis. Our resonance parameters for two levels are in good agreement with the results of previous studies, while for four others, excitation energy, proton partial width, and spin-parity assignment disagree with the results of recent study via elastic scattering of $^{25}\mathrm{Al}+p$.

Conclusion: The parameters of resonant states in ^{26}Si determined in the present work for the $^{25}\mathrm{Al}(p,\gamma)^{26}\mathrm{Si}$ reaction rate are consistent with that of the previous result, solving spin-parity assignment discrepancies between experiments, relevant at higher temperatures.

DOI: 10.1103/PhysRevC.90.035805 PACS number(s): 24.30.−v, 25.40.Cm, 26.30.−k, 27.30.+t

I. INTRODUCTION

The $^{25}\mathrm{Al}(p,\gamma)^{26}\mathrm{Si}$ reaction is relevant to the production of galactic $^{26}\mathrm{Al}^{\mathrm{gs}}$ ($t_{1/2}=0.717\times10^{6}$ y), which is a piece of evidence implying that galactic nucleosynthesis is an ongoing process [1,2]. The ground state of ^{26}Al decays to the first excited state in ^{26}Mg, giving rise to a 1.809-MeV γ ray which has been observed with satellite-based γ-ray observatories [3]. The main reaction sequence leading to the production of $^{26}\mathrm{Al}^{\mathrm{gs}}$ is $^{24}\mathrm{Mg}(p,\gamma)^{25}\mathrm{Al}(\beta^{+}\nu)^{25}\mathrm{Mg}(p,\gamma)^{26}\mathrm{Al}$. However, if the $^{25}\mathrm{Al}(p,\gamma)^{26}\mathrm{Si}$ reaction becomes faster than the competing decay of ^{25}Al at temperatures of typically >0.5 GK expected for shell carbon burning and explosive neon burning, the reaction sequence $^{25}\mathrm{Al}(p,\gamma)^{26}\mathrm{Si}(\beta^{+}\nu)^{26}\mathrm{Al}^{m}(\beta^{+}\nu)^{26}\mathrm{Mg}^{\mathrm{gs}}$ bypasses $^{26}\mathrm{Al}^{\mathrm{gs}}$, and no 1.809-MeV γ rays are emitted. Therefore, the proton capture on ^{25}Al might lead to a destruction of the ground state of ^{26}Al under high-temperature conditions. In principle, internal transitions (γ decay) from the isomer ($^{26}\mathrm{Al}^{m}$) to the ground state ($^{26}\mathrm{Al}^{\mathrm{gs}}$) are forbidden by their large spin difference ($\Delta J=5$). However, if the $^{26}\mathrm{Al}^{m}$ can communicate with the $^{26}\mathrm{Al}^{\mathrm{gs}}$ through the thermal population of excited levels above the critical temperature of $T=0.4$ GK [4–6], then this thermal process would enhance the production of $^{26}\mathrm{Al}^{\mathrm{gs}}$. Therefore, the destruction of ^{25}Al by proton capture is an essential path for the production of $^{26}\mathrm{Al}^{\mathrm{gs}}$. Consequently, the $^{25}\mathrm{Al}(p,\gamma)^{26}\mathrm{Si}$ reaction rate needs to be determined accurately to estimate the production of $^{26}\mathrm{Al}^{\mathrm{gs}}$ at higher temperatures.

The level structure of ^{26}Si is also key to understanding the nucleosynthesis and energy generation, because it plays a role in the calculation of $^{25}\mathrm{Al}(p,\gamma)^{26}\mathrm{Si}$ reaction rate. This reaction itself is important for understanding explosive hydrogen burning environments like novae and x-ray bursts. Thermonuclear runaway is driven mostly by the rapid proton capture process (rp process) and the αp process that is responsible for building up of heavier elements, especially proton-rich nuclides [7,8]. For higher-temperature environments, for example, the atmosphere of an accreting neutron stars [7], the reaction flow is driven by the αp process. However, above $Z=20$ the Coulomb barrier reduces the α-capture reaction rates, which leads to a termination of the αp process. The thermonuclear runaway above $Z=20$ is predicted to be entirely driven by the rp process. Model simulations show that $^{25}\mathrm{Al}(p,\gamma)^{26}\mathrm{Si}$ is activated along the rp-process paths in explosive hydrogen burning [9,10]. This reaction takes place mostly through resonant states of the compound nucleus ^{26}Si, making the reaction rates very sensitive to the level structure of the relevant resonances in ^{26}Si.

So far, a number of studies have been made to investigate the contributions to the reaction rate on the basis of limited experimental data and shell-model calculations. There are, however, large uncertainties regarding the level structure of ^{26}Si [11–14], especially for higher-lying resonances. To reduce the uncertainties, the structure of ^{26}Si has been studied with various reactions such as (p,t) [15–17], $(^{3}\mathrm{He},n)$ [18,19], $(^{4}\mathrm{He},^{6}\mathrm{He})$ [20], and (p,p) [21], as well as the observation of protons and γ which are products of β decays [22]. Although many states above the proton-emission threshold have been discovered, conflicting spin and parity assignments have been made and varying subsets of states, at energies corresponding to higher temperatures ($T>0.4$ GK), have been identified in the various studies. Moreover, a comparison with its mirror nucleus ^{26}Mg indicates that missing states still remain.

In the present study, we measured the excitation function over the excitation energy E_x range of 6.6–8.3 MeV in ^{26}Si by the resonant elastic scattering of $^{25}\mathrm{Al}+p$, which has been frequently used to study proton resonances in proton-rich unstable nuclei [23–25]. If a resonance state exists with a sufficiently large width, it can be identified in the excitation function as an interference pattern of potential and resonance scattering, and its resonance parameters such as excitation energy, proton partial width, and spin parity can be determined as well. The excited states of ^{26}Si in this energy region have previously been studied via elastic proton scattering and were published by Chen *et al.* [21]. However, owing to low statistics and background contamination, which originated from the beam interacting with carbon atoms in the CH_2 target in an energy region where the prominent resonances are located (see Fig. 3 of Chen *et al.* [21]), the experimental resonance parameters have large uncertainties. As a result, the excitation function had a limited resolution and the background substraction caused a systematic uncertainty. The goal of the present measurement was to study the high-lying states in ^{26}Si over a broad range within the Gamow window ($E_x\sim6$–8 MeV at $T_9=0.4$–5), as well as to reduce uncertainties in their parameters. Background contamination was removed by replacing the CH_2 solid target with a pure hydrogen gas target, and sufficient statistics were obtained to perform a reliable analysis.

II. EXPERIMENTAL PROCEDURE

The measurement of the $^{25}\mathrm{Al}+p$ elastic scattering was performed in inverse kinematics [26] at the low-energy radioactive ion (RI) beam facility Center for Nuclear Study Radioactive Ion Beam separator (CRIB) [27,28], using the thick target method. The experimental setup is identical to the one used in our previous study of the $^{26}\mathrm{Si}+p$ elastic scattering [29]. An ^{25}Al RI beam can be produced at CRIB

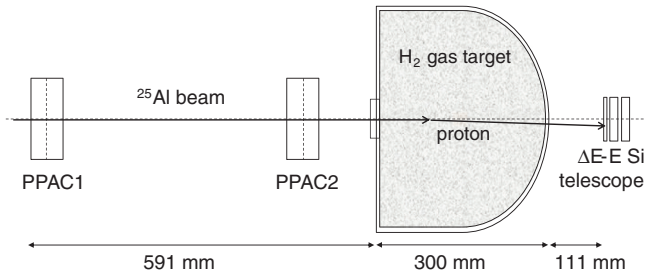

FIG. 1. Experimental setup of the measurement of the ^{25}Al + p elastic scattering in inverse kinematics at the final focal plane following the Wien filter.

by the in-flight method using a cryogenic gas target [30]. In the present measurement, an ^{25}Al beam was produced via the ^{3}He(^{24}Mg,^{25}Al)d reaction using a ^{3}He gas target at 550 Torr and a ^{24}Mg beam with an energy of 7.5 MeV/nucleon extracted from an azimuthally varying field (AVF) cyclotron. The ^{25}Al beam was separated and purified by magnetic analysis and velocity selection with a Wien filter. The beam, with a purity of about 62% and an intensity of 3.3×10^4 pps, was delivered to the reaction target located at the F3 focal plane. Two parallel-plate avalanche counters (PPACs) [31] were used for detection of the incoming beam position and timing. The experimental setup following the Wien filter is shown in Fig. 1.

The reaction target was a thick hydrogen gas target, at a pressure of 330 Torr, housed in a 300-mm-radius semicylindrical shape, and sealed with a 2.5-μm-thick Havar foil as a beam entrance window and with a 25-μm-thick aluminized Mylar foil as an exit window. The ^{25}Al beam energy after the entrance window of the hydrogen gas target was measured as 71.58 ± 0.54 MeV with a single-pad silicon detector covered by a thin (2.5 μm) Havar foil having the same thickness as the entrance window. The beam lost energy while passing through the thick gas target. Therefore, using one incident beam energy, the cross section at various energies was measured simultaneously [32,33]. Another feature is that, compared to the solid CH_2 target, the pure hydrogen gas target is free from background contributions. Last, using a thick target makes a large difference to the time of flight between resonant elastic and inelastic scattering events passing through the target, owing to the different velocities of beam and recoiling protons. This feature could be used to separate the elastic and inelastic scattering events.

Protons elastically scattered to forward angles were detected by a ΔE-E telescope, which consisted of a 75-μm-thick double-sided position-sensitive silicon detector (PSD), with 16×16 strips, and two 1500-μm-thick single-channel silicon strip detectors (SSDs), both with an active area of 50×50 mm^2. The telescope was placed at a distance of $\sim$400 mm from the entrance of the target at $\theta_{\rm lab} = 0^\circ$. These detectors were calibrated separately with α sources, and a further calibration was performed with proton beams at various energies for the ΔE-E telescope during the run. High-energy protons originating upstream of the scattering chamber could be eliminated by vetoing events from the second SSD because the energy of the recoil protons was so high that they punch through the PSD (ΔE), but were stopped in the first SSD (E). Proton events were selected by using the energy measured from the ΔE-E detector and timing information between the PPAC and the SSD (E). Shown in Fig. 3 is a two-dimensional plot of the total energy deposition versus energy deposition in the PSD (ΔE) (left panel), as well as the time-of-flight (TOF) versus total energy deposition (right panel).

III. EXPERIMENTAL RESULTS

The energy of the scattered proton measured by the ΔE-E detector was converted into a center-of-mass energy ($E_{\rm c.m.}$) using the kinematical relationship for elastic scattering,

$$E_{\rm c.m.} = \frac{M_{\rm Al} + M_p}{4M_{\rm Al}\cos^2\theta_{\rm lab}} E_p, \qquad (1)$$

where $M_{\rm Al}$ and M_p are the nuclear masses of the heavy ^{25}Al beam particle and the scattered proton, respectively, E_p is the measured energy of the scattered protons in the laboratory frame, and $\theta_{\rm lab}$ is the scattering angle between the proton and the beam particle. Proton events were selected in coincidence with an ^{25}Al beam particle measured by a PPAC. The scattering angle was determined from the detection position of two PPACs and the ΔE-E detector. The energy loss of the scattered proton in the thick-target, along with an ^{25}Al beam particle, was calculated by the SRIM code [34] and used for the kinematics conversion process.

Figure 2 shows the proton spectrum for ^{25}Al + p elastic scattering in the center-of-mass frame after the complete conversion. Prominent resonance peaks are clearly seen, and the positions of these peaks are essentially in good agreement with previous results [21]. The differential cross section $d\sigma/d\Omega$ was calculated for each small energy division using the number of selected proton events and incident beam particles, the effective target thickness, and the different solid angles of the detector, depending on the reaction position in the thick target. The solid angle was calculated by the geometrical

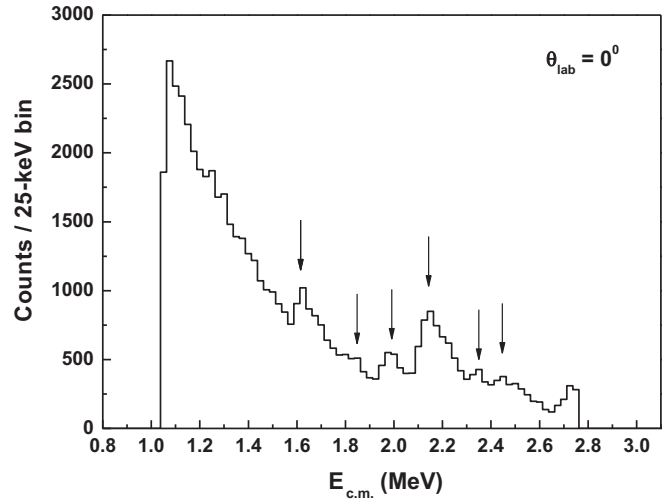

FIG. 2. Energy spectrum of proton for ^{25}Al + p elastic scattering after conversion to the center-of-mass frame at $\theta_{\rm lab} = 0^\circ$. Arrows indicate the prominent resonance states.

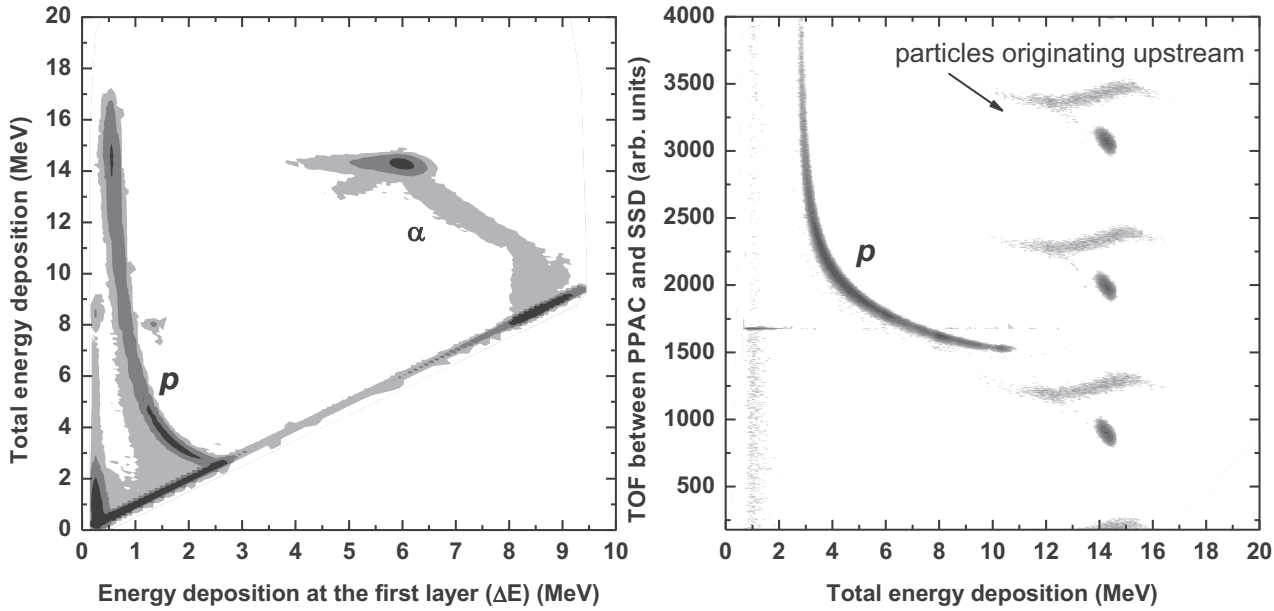

FIG. 3. ΔE-E plot (left) and two-dimensional plot of TOF vs total energy deposition (right) for the particle identification.

information of the detector and the reaction position in the target determined by the kinematical calculation. Corresponding excitation energies in ^{26}Si were obtained through the relation that $E_x = E_{\mathrm{c.m.}} + 5.5135$ MeV [21], the threshold energy of which was determined from a weighted average of recent results. The overall uncertainty (1σ width of a Gaussian distribution) in $E_{\mathrm{c.m.}}$ of the excitation function was estimated as 26–31 keV, depending on the energy ($E_{\mathrm{c.m.}}$). The uncertainty originated mainly from the energy straggling of the ^{25}Al beam and the protons passing through the target and windows, the energy resolution of the ΔE-E detector, and the angular uncertainty owing to the finite size of the detector and the distance of the scattering location within the thick, extended target. The energy straggling was calculated by the code ATIMA [35] with a 1σ width of a Gaussian distribution. The energy resolution of the detector was obtained by fit with a Gaussian function, and angular uncertainty was estimated using the geometrical relation. Finally, the overall uncertainty was estimated by an error propagation.

Because the proton spectrum was obtained under the assumption of kinematics describing only the elastic scattering of $^{25}\mathrm{Al} + p$, the resonant elastic and inelastic scattering events should be clearly separated. The first excited state in ^{25}Al is at 450 keV with a $J^\pi = 1/2^+$, which is at least energetically allowed to make a proton decay from the populated ^{26}Si resonant states. However, the first excited-state population by proton d-wave or g-wave transitions from the resonant states is largely hindered by the low Coulomb penetration probabilities owing to larger l and smaller $E^{\mathrm{inel}}_{\mathrm{c.m.}}(p) = E_{\mathrm{R}} - E_x(^{25}\mathrm{Al})$. In addition, the resonant states obtained in the present work over the energy range of 7.0–8.0 MeV decay to the ground state of ^{25}Al via the β-delayed protons, as shown in Fig. 13 of Thomas *et al.* [22]. Therefore, the contribution of the inelastic scattering is considered to be negligible. To identify the different types of proton scattering (elastic vs inelastic), a two-dimensional plot of the TOF between the first PPAC and the SSD versus the proton energy was used, the same method which was applied to our previous study [29]. The beam travels slower than recoiling protons within the target and protons have different flight times depending on the position in the target and type of scattering. This enables elastic-scattering events to be separated from the background sources such as the excited states of ^{25}Al, the exit window of the target, the PPACs, which contain hydrogen, and other upstream sources. According to the 2D plot [see Fig. 3 (right)], no evident inelastic structure was seen. We conclude that the scattering should mostly correspond to the ground state of ^{25}Al.

IV. *R*-MATRIX ANALYSIS AND DISCUSSION

Several resonance structures were clearly observed in our proton spectrum, as shown in Fig. 4: two prominent peaks at 1.6 and 2.0 MeV, a small peak around 1.9 MeV, a strong peak around 2.1 MeV, a small bump at 2.3 MeV, and a broad peak at 2.5 MeV. The differential cross-section data were examined by R-matrix analysis (SAMMY-8.0.0) [36,37] to extract resonance parameters such as excitation energy E_x, spin J, parity π, and proton partial width Γ_p of the resonance states obtained in the present work. We chose the reaction-channel radius given by Ref. [21],

$$r_c = 1.2\left(A_t^{1/3} + A_p^{1/3}\right)\ \mathrm{fm}, \tag{2}$$

where A_t and A_p are the mass numbers of the target and projectile, respectively, as one of the input parameters. The fit result was found to be insensitive to changes in the channel radius. A best result was obtained after attempting many R-matrix fits with all possible spin-parity combinations (see below) for the observed resonances. The energy broadening owing to the experimental resolution was considered in the R-matrix calculations.

The possible combinations of channel spins, relative orbital angular momentum, and spin-parities of the compound nucleus

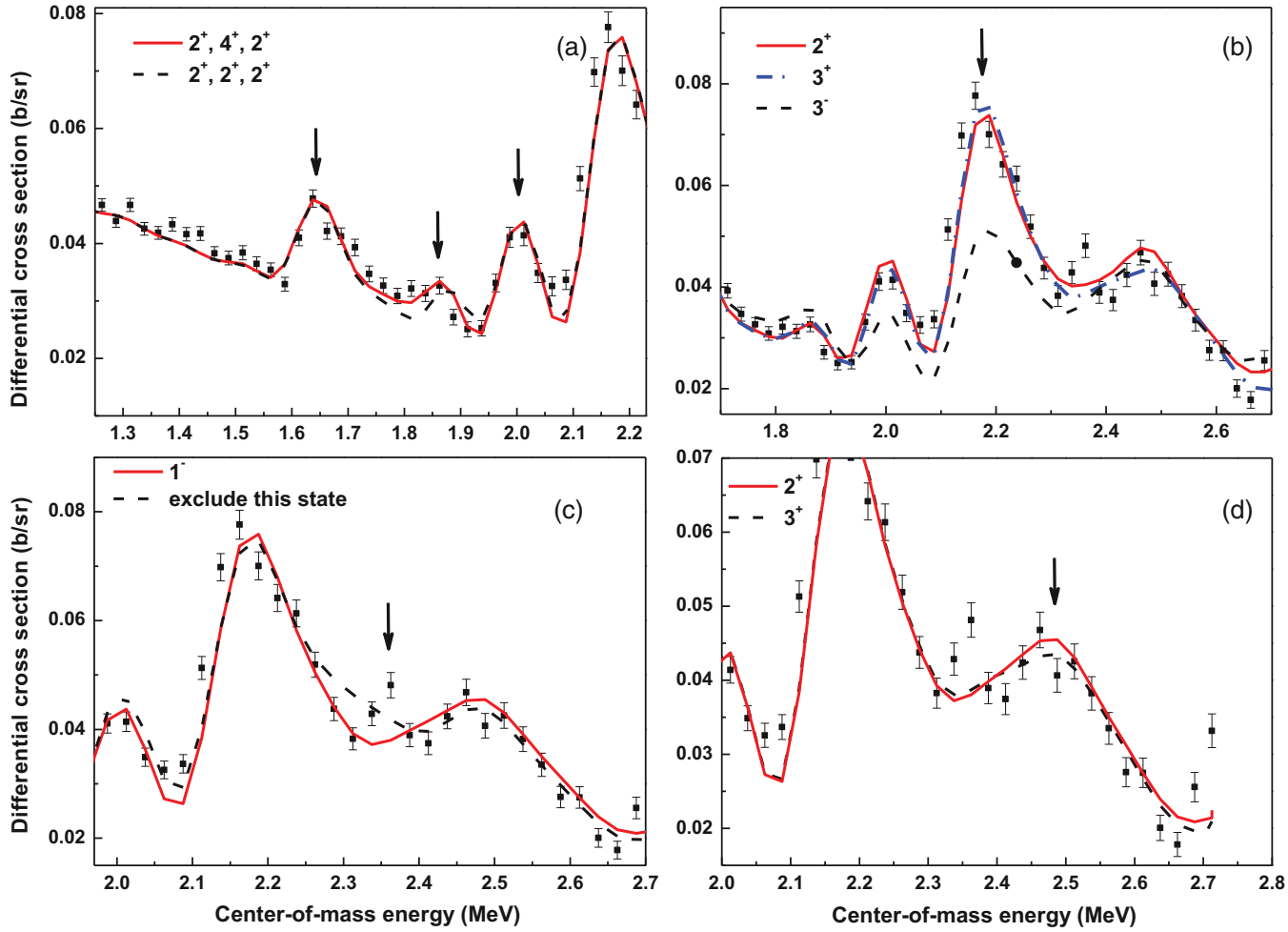

FIG. 4. (Color online) Excitation function for ^{25}Al + p elastic scattering cross section fitted by the R-matrix calculation. The arrows correspond to structures discussed in Sec. IV.

are derived from conservation of total angular momentum before and after the scattering. Because the spin parity of the proton is $J^\pi = 1/2^+$ and that of the ground state of ^{25}Al is $5/2^+$, the incident channel spin is $S = 1/2 \oplus 5/2 = 2$ or 3. Therefore, allowed spin parities of the compound nucleus, ^{26}Si, are assigned as $J^{(-1)^l}$, where $J = l \oplus S$ and l is the relative orbital angular momentum of the proton with respect to the nucleus. To cope with the many fitting parameters, for initial input parameters we adopted the resonance parameters, such as level energies and spin-parity assignments, from previous measurements [15–17,20–22]. The R-matrix analysis is the preferred method for spin-parity assignment because other methods, such as the DWBA and Hauser-Feshbach analysis are associated with strong model dependencies.

Figure 5 shows the best-fit result for the excitation function of ^{25}Al + p elastic scattering. The best-fit parameters are summarized in Table I and the corresponding level energies and spin parities in comparison with those from previous studies are given in Table II. The uncertainty in energy includes both systematic and fitting uncertainty. In the following, the detailed discussions for each state are presented.

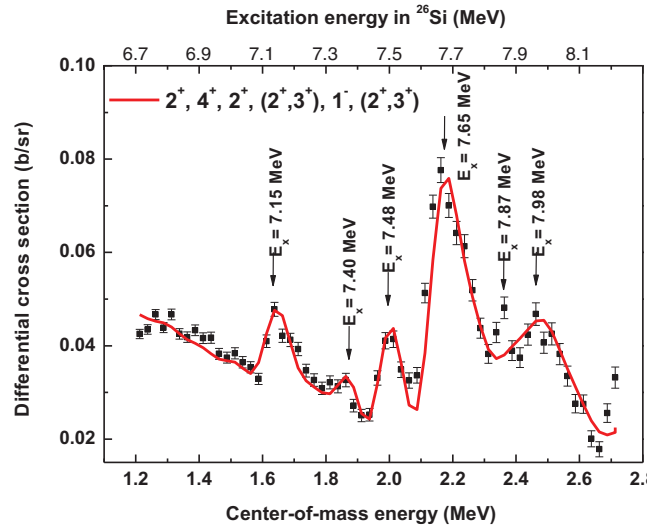

FIG. 5. (Color online) The best-fit curve for $J^\pi = 2^+$, 4^+, 2^+, (2^+ or 3^+), 1^-, and (2^+ or 3^+) is shown but without firm spin-parity assignments for the fourth and sixth resonant peaks correctly. Corresponding excitation energy in ^{26}Si is $E_x = E_{\text{c.m.}} + 5.5135$ MeV.

TABLE I. Best-fit resonance parameters of ^{25}Al and resonance strengths for the ^{25}Al$(p,\gamma)^{26}$Si reaction rate obtained in the present work. Spin parities for the resonant states at 2.140 and 2.463 MeV are put in parentheses, which means they are tentative assignments.

$E_{\text{c.m.}}$ (MeV)	E_x (MeV)	J^π	l	Γ_p [a] (keV)	Γ_p [b] (keV)	Γ_γ [c] (eV)	$\omega\gamma$ (eV)
1.633(27)	7.147	2^+	0	2.7 ± 0.1	10.0	1.00×10^{-2}	4.17×10^{-3}
1.887(28)	7.401	4^+	2	1.1 ± 0.1	4.1	1.00×10^{-2}	7.49×10^{-3}
1.970(28)	7.484	2^+	0	15.9 ± 0.3	28.0	1.00×10^{-2}	4.17×10^{-3}
2.140(29)	7.654	$(2^+,3^+)$	0	$(30.1 \pm 0.5, 19.5 \pm 0.3)$		1.00×10^{-2}	4.17×10^{-3}
2.352(29)	7.866	1^-	1	22.8 ± 1.3		5.17×10^{-1}	1.29×10^{-1}
2.463(30)	7.977	$(2^+,3^+)$	0	$(4.5 \pm 0.3, 3.6 \pm 0.2)$		1.00×10^{-2}	5.83×10^{-3}

[a]The error evaluation of Γ_p is simply by the statistical error from the R-matrix fit procedure and thus could be underestimated.
[b]Theoretically calculated Γ_p values, taken from Ref. [39]. The calculation is based on the USDB Hamiltonian.
[c]Γ_γ values are taken from Ref.[15].

A. Peaks at 1.63 and 1.97 MeV

Because nonresonant scattering is dominant at low energies below ∼1.5 MeV, no clear resonance was observed in the excitation function over this energy region, as shown in Fig. 4(a). However, as three states at $E_x = 6.786$, 6.880, and 7.147 MeV in this energy region have been studied before, such a flat structure was reproduced well by using the previous parameters determined by Matic *et al.* [15]. Thus, the resonance parameters of lower energy states were fixed while those of prominent peaks were taken as free parameters for the R-matrix analysis.

The lowest resonance peak observed around 1.63 MeV ($E_x = 7.147$ MeV) was reproduced well by the R-matrix calculation with a $J^\pi = 2^+$ assignment. This is in good agreement with previously reported assignment for this resonance level from transfer reaction studies [15–17,19,20] and proton resonant scattering experiment [21]. The 1.97-MeV resonance ($E_x = 7.484$ MeV) was also well fitted by a $J^\pi = 2^+$ assignment. Both the spin-parity assignment and the level energy are in good accord with previously reported results [15–17,19–21].

B. Peak at 1.89 MeV

The small peak around 1.89 MeV ($E_x = 7.401$ MeV) was fitted best with a $J^\pi = 4^+$ assignment. The most recent study by Chen *et al.* [21] suggested a $J^\pi = 2^+$ assignment, which was adopted from Bardayan *et al.* [16] and Chipps *et al.* [17]; however, it was difficult to confirm because the poor statistics in their experiment resulted in a relatively large uncertainty in the resonance parameters of this level. An additional complication in their experiment stemmed from background, arising through either scattering or reactions on carbon in the target and potentially leading to minor (though relevant) modifications of the shape or size of such a small resonance peak. However, background substraction was reasonably performed (see Fig. 3 in Ref. [21]). Although, as shown in Fig. 4(a), fitting our experimental data with $J^\pi = 2^+$ shows less agreement with the peak heights than fitting with $J^\pi = 4^+$. Based on the observed angular distribution (Fig. 6 of Ref. [15]), Matic *et al*. also deduced a $J^\pi = 4^+$ assignment for this level. However, the $J^\pi = 4^+$ assignment does disagree with the $J^\pi = 0^+$ assignment suggested by Bohne *et al.* [18]

TABLE II. Excitation energies E_x (MeV) and spin parities J^π for levels in ^{26}Si in the range of 7.1 to 8.2 MeV from the present work and in comparison with those of previous studies.

Present (p,p)	Ref. [21][a] [15][b] (p,p)	Ref. [19]. (p,t)	Ref. [22][c] β^+ decay	Ref. [19][d] (^{3}He,n)
7.147(27), 2^+	7.162(14), 2^+	7.151(5), 2^+		7.152(4), 2^+
7.401(28), 4^+	7.402(40), 2^+	7.415(23), (4^+)		7.425(4), 0^+
7.484(28), 2^+	7.484(13), 2^+	7.479(12), 2^+	7.501(5), 2^+	7.493(4), 2^+
			7.606(6)	
		7.522(12), (5^-)		
7.654(29), $(2^+,3^+)$		7.661(12), (2^+)		
	7.704(13), 3^+	7.701(12), 3^-		7.694(4), 3^-
7.866(29), 1^-		7.874(4), 1^-		7.899(4), 1^-
			7.962(5)	
7.977(30), $(2^+,3^+)$	8.015(14), 3^+			
		8.120(3), 2^+ [e]	8.156(21), 2^+	

[a]J^π from a R-matrix analysis.
[b]J^π from a mirror assignments and Ref. [19].
[c]J^π from a β-decay property study comparing with shell-model calculations.
[d]J^π from a Hauser-Feshbach analysis.
[e]Weighted average of E_x and J^π from a mirror assignment.

on the basis of the DWBA and the Hauser-Feshbach analysis by Parpottas *et al.* [19].

C. Peak at 2.14 MeV

Compared to the proton elastic scattering study performed by Chen *et al.* [21], the overall shapes of the two excitation functions do have a similar configuration. However, we observe clearly the strong resonance at around 2.14 MeV ($E_x = 7.654$ MeV) with a higher differential cross section. Attempts were made to fit the peak with $J^\pi = 2^+$, 3^+, and 3^-, which were assignments that had been made by previous measurements [18,28,30,32]. In the previous study [21], this state was observed at $E_x = 7.704(13)$ MeV, suggesting that it could be identified with the $E_x = 7.701$-MeV state of Ref. [15], but they assigned the spin and parity as $J^\pi = 3^+$, not 3^-. As shown in Fig. 4 of Ref. [21], the fit for $J^\pi = 3^+$ provided the best fit while fits with both $J^\pi = 2^+$ and 3^-, showing a similar pattern, were not satisfactory. On the other hand, our result shows that the best fit was obtained with $J^\pi = 2^+$ or 3^+, both of which are consistent with our data, while $J^\pi = 3^-$ was wholly unsatisfactory at reproducing our data, as shown in Fig. 4(b). Most of previous studies have confirmed this state to have an assignment of $J^\pi = 3^-$ and excitation energies of $E_x = 7.672(2)$ [17], 7.701(12) [15], 7.687(22) [16], and 7.694(4) [19] have been reported. In the recent high-resolution study performed by Matic *et al.* [15], however, a new state at $E_x = 7.661(12)$ MeV was measured. It was given a $J^\pi = 2^+$ assignment on the basis of the mirror nucleus. Because fitting the present experimental data with a $J^\pi = 3^-$ yields a poor description of the data, and because our excitation energy of $E_x = 7.654$ MeV has been extracted using either a $J^\pi = 2^+$ or 3^+ assignment, we suggest that our state could be identified as the 7.661-MeV state in Ref. [15], with a $J^\pi = 2^+$ assignment. Furthermore, two states at $E_x = 7.661(12)[2^+]$ and 7.701(12) MeV [15] in this region can be considered as a doublet. To investigate this we calculated the fit for the level assuming two states; however, there was no difference in the fit between using a single or a doublet state.

D. Small structure at 2.35 MeV

A resonance representing a small bump around 2.35 MeV ($E_x = 7.866$ MeV) in the middle of the two prominent peaks was included in the R-matrix calculation. Exclusion of this bump resulted in a less satisfactory fit for the tail of the most prominent peak around 2.14 MeV, as shown in Fig. 4(c). To improve the fitting we introduced one resonance at this region, and data were fitted by using an assignment of $J^\pi = 1^-$ for this state, which was adopted from previous reports, corresponding to the state at $E_x = 7.875(2)$ [17], 7.874(4) [15], 7.900(22) [16], 7.899(4) [19]. However, it was difficult to derive conclusive resonance parameters for such a small peak with the current systematic energy resolution. According to the nearby resonance states from previous studies [15–17,19,21], other plausible assignments for this state are $J^\pi = 3^+, 3^-$, and 2^+. Curves calculated with these assignments totally deviate from the data, however. Therefore, we reject these possible cases and take a $J^\pi = 1^-$ for this resonance.

E. Peak at 2.46 MeV

Last, the resonance around 2.46 MeV ($E_x = 7.977$ MeV) was fitted well with $J^\pi = 2^+$ or 3^+, as shown in Fig. 4(d). We adopted the $J^\pi = 2^+$ assignment from Refs. [18,22] and also the $J^\pi = 3^+$ from Refs. [15,21]. In the β-delayed proton decay study [22], two states in this energy region were measured $E_x = 7.962(5)$ and 8.156(21) MeV. The β-delayed one proton of the ^{26}Si proton-unbound excited state at $E_x = 7.962$ MeV decays towards the second excited state in ^{25}Al (see Fig. 13 of Ref. [22]). This level is unlikely to correspond to our resonance at $E_x = 7.977(30)$ MeV because we identified that the resonance is from elastic scattering by TOF. Thus, one possible suggestion is that our state could be identified as the previous 8.156-MeV state [22] or the 8.120-MeV state [18] with an assignment of $J^\pi = 2^+$, but there is a discrepancy in the excitation energies between the previous and the present studies.

Another possibility is that this state may correspond to a level at 2.501 (14) MeV ($E_x = 8.015$ MeV) [21] that has been newly observed. An assignment of $J^\pi = 3^+$ has been suggested, based on both an R-matrix fit and the possible mirror assignment proposed by Matic *et al.* [15]. Because there is a difference in the energy, we would suggest that resonance parameters for this level should be replaced with our results. For this resonance, however, we propose a spin-parity assignment of either $J^\pi = 2^+$ or 3^+. There was very little influence on the fit from either assignment.

V. ASTROPHYSICAL IMPLICATIONS FOR THE ^{25}Al(p,γ)^{26}Si REACTION

The resonances observed in the present work might contribute to the astrophysical ^{25}Al(p,γ)^{26}Si reaction rate at high temperature, $T > 0.5$ GK. We have calculated the resonance strengths for the ^{25}Al(p,γ)^{26}Si reaction based on the obtained ^{26}Si excitation energies, spin-parities, and proton partial widths in the present study. The relevant parameters are listed in Table I. The γ partial widths Γ_γ for levels are taken from Matic *et al.* [15]. For the 2.352-MeV 1^- resonance, the calculated Γ_γ value was taken from half-life data for the ^{26}Mg mirror nucleus [38]. For the 2.140- and 2.463-MeV resonances, tentative assignments of $J^\pi = 2^+$ and 3^+, respectively, have been used in accordance with suggestions from Ref. [15].

There have been inconsistent assignments for the spin and parities of the high-lying levels at around $E_x = 7.4$, 7.6, and 8.0 MeV (see Table II), which significantly influence the astrophysical ^{25}Al(p,γ)^{26}Si reaction rate at higher-temperature conditions. By performing a new measurement, more reliable assignments were made, which were in the end fully consistent with that of Matic *et al.* [15]. Therefore, our results support the reaction rate evaluated by Matic *et al.*, providing further evidence for the spin-parity assignments.

Because we did not observe a significant contribution of Γ_p to the resonance strength (see Table I), $\Gamma_{\text{total}} = \Gamma_p + \Gamma_\gamma \sim \Gamma_p$ and the reaction rate is primarily independent of Γ_p. Nevertheless, the Γ_p we determined is important as nuclear information as well as spin-parity assignments.

VI. CONCLUSION

We have studied the resonant elastic scattering of $^{25}\mathrm{Al} + p$ using an RI beam at CRIB. Our experiment has the distinct advantage over previous ones owing to the use of a pure hydrogen target, which removes background contributions in the target, as well as better statistics.

The excitation function for the cross section of ^{26}Si was measured by the thick-target method in inverse kinematics. Six resonant states in ^{26}Si have been observed, and we mostly determined and brought new information on their resonance parameters such as resonance energy, proton partial width, and spin-parity with an R-matrix calculation. Compared to the previous resonant proton scattering study [21], we found differences in the cross section and the energy in the excitation functions, although their spectral shapes are mostly consistent with each other. In addition, our resonance parameters for three levels in the excitation-energy range from 7.1 and 7.5 MeV are in good agreement except for the spin-parity assignment of the state at $E_x = 7.401$ MeV. The remaining three states at higher excitation energy ($E_x = 7.6$–8.0 MeV) have resonance parameters that disagree with those of previously observed states. This discrepancy might be related to the background contribution from reactions on the carbon in the CH_2 target, which were strongly distributed around this energy region [21].

We succeeded in making more reliable assignments on the spin parities for levels above $E_x = 7.4$ MeV and confirmed that evaluations of the $^{25}\mathrm{Al}(p,\gamma)^{26}$Si reaction rate by Matic *et al.* [15] was reasonable at higher temperatures. However, compared to the mirror nucleus ^{26}Mg, a number of states in ^{26}Si have yet to be observed. As a consequence of the incomplete structure, knowledge of ^{26}Si and the $^{25}\mathrm{Al}(p,\gamma)^{26}$Si reaction rate in that temperature range still depends on statistical model (Hauser-Feshbach) predictions. More studies are favored for the determination of resonant parameters at higher temperatures, $\geqslant 1$ GK.

ACKNOWLEDGMENTS

The experiment was performed at RI Beam Factory operated by RIKEN Nishina Center and CNS, University of Tokyo. We are grateful to the CNS and RIKEN accelerator staff for their help. This work was supported by the National Research Foundation Grant funded by Korea Government (Grants No. NRF-2009-0093817 and No. NRF-2013R1A1A2063017), by National Nuclear R&D Program (Grant No. 2010-0023862) through the National Research Foundation of Korea, by KAKEHI of Japan (Grants No. 21340053 and No. 25800125), and by the Korea-Japan Joint Research Project through NRF and JSPS.

[1] W. A. Mahoney, J. C. Ling, A. S. Jacobson, and R. Lingenfelter, Astrophys. J. **262**, 742 (1982).
[2] N. Prantzos and R. Diehl, Phys. Rep. **267**, 1 (1996).
[3] R. Diehl *et al.*, Astron. Astrophys. **298**, 445 (1995).
[4] R. A. Ward and W. A. Fowler, Astrophys. J. **238**, 266 (1980).
[5] A. Coc, M.-G. Porquet, and F. Nowacki, Phys. Rev. C **61**, 015801 (1999).
[6] R. C. Runkle, A. E. Champagne, and J. Engel, Astrophys. J. **556**, 970 (2001).
[7] R. K. Wallace and S. E. Woosley, Astrophys. J. Suppl. **45**, 389 (1981).
[8] A. E. Champagne and M. Wiescher, Annu. Rev. Nucl. Part. Sci. **42**, 39 (1992).
[9] A. Parikh, J. José, F. Moreno, and C. Iliadis, Astrophys. J. Suppl. Ser. **178**, 110 (2008).
[10] J. L. Fisker, H. Schatz, and F.-K. Thielemann, Astrophys. J. **174**, 261 (2008).
[11] M. Wiescher, J. Görres, F.-K. Thielemann, and H. Ritter, Astron. Astrophys. **160**, 56 (1986).
[12] C. Iliadis, L. Buchmann, P. M. Endt, H. Herndl, and M. Wiescher, Phys. Rev. C **53**, 475 (1996).
[13] C. Iliadis, J. D'Auria, S. Starrfield, W. Thompson, and M. Wiescher, Astrophys. J. Suppl. **134**, 151 (2001).
[14] C. Wrede, Phys. Rev. C **79**, 035803 (2009).
[15] A. Matic *et al.*, Phys. Rev. C **82**, 025807 (2010).
[16] D. W. Bardayan *et al.*, Phys. Rev. C **65**, 032801 (2002).
[17] K. A. Chipps *et al.*, Phys. Rev. C **82**, 045803 (2010).
[18] W. Bohne *et al.*, Nucl. Phys. A **378**, 525 (1982).
[19] Y. Parpottas *et al.*, Phys. Rev. C **70**, 065805 (2004).
[20] Y. K. Kwon *et al.*, J. Korean Phys. Soc. **53**, 1141 (2008).
[21] J. Chen *et al.*, Phys. Rev. C **85**, 015805 (2012).
[22] J.-C. Thomas *et al.*, Eur. Phys. J. A **21**, 419 (2004).
[23] R. Coszach *et al.*, Phys. Rev. C **50**, 1695 (1994).
[24] A. Galindo-Uribarri *et al.*, Nucl. Instrum. Methods B **172**, 647 (2000).
[25] T. Teranishi *et al.*, Phys. Lett. B **556**, 27 (2003).
[26] K. P. Artemov *et al.*, Sov. J. Nucl. Phys. **52**, 408 (1990).
[27] S. Kubono *et al.*, Eur. Phys. J. A **13**, 217 (2002).
[28] Y. Yanagisawa *et al.*, Nucl. Instrum. Methods Phys. Res., Sect. A **539**, 74 (2005).
[29] H. S. Jung *et al.*, Phys. Rev. C **85**, 045802 (2012).
[30] H. Yamaguchi *et al.*, Nucl. Instrum. Methods Phys. Res., Sect. A **589**, 150 (2008).
[31] H. Kumagai *et al.*, Nucl. Instrum. Methods Phys. Res., Sect. A **470**, 562 (2001).
[32] W. Galster *et al.*, Phys. Rev. C **44**, 2776 (1991).
[33] S. Kubono, Nucl. Phys. A **693**, 221 (2001).
[34] J. F. Ziegler, *The Stopping and Rannges of Ions in Matter*, Vols. 3 and 5 (Pergamon Press, Oxford, 1980).
[35] O. B. Tarasov and D. Bazin, Nucl. Instrum. Methods Phys. Res., Sect. B **266**, 4657 (2008).
[36] A. M. Lane and R. G. Thomas, Rev. Mod. Phys. **30**, 257 (1958).
[37] N. Larson, A Code System for Multilevel R-Matrix Fits to Neutron Data Using Bayes' Equations, ORNL/TM-9179/R5, 2000 (unpublished).
[38] P. M. Endt, J. Blachot, R. B. Firestone, and J. Zipkin, Nucl. Phys. A **633**, 1 (1998).
[39] W. A. Richter, B. A. Brown, A. Signoracci, and M. Wiescher, Phys. Rev. C **83**, 065803 (2011).